Suplemento de la Revista Mexicana de Física **1** (2) 25–33 JUNE–JULY 2020

Permeability simulation in an elastic deformable sandstone under stress changes

M. E. Vadillo-Sáenz, P. F. Aguilar-Gastelum, M. A. Díaz-Viera, and M. Coronado
Instituto Mexicano del Petróleo,
Eje Central Lázaro Cárdenas Norte 152, San Bartolo Atepehuacán,
Gustavo A. Madero, 07730, Ciudad de México, México.

Received 3 March 2020; accepted 1 April 2020

Fluid flow and rock mechanics become coupled in various important phenomena in Geosciences. In order to study this coupling, laboratory work has been carried out in triaxial cells along the years for various rock and fluid types at different confinement stress and pore pressure conditions. In a similar way, poromechanic models have been developed to simulate them, in which constitutive porosity and permeability correlation models in terms of strain, stress and fluid pressure have to be provided. However, to date, the applicability of the available correlation models to describe this phenomenon in different types of rock remains to be analyzed. In this work, a single-phase poroelastic model is applied to simulate a published geomechanical test performed in sandstones to examine the capacity of commonly used constitutive porosity and permeability correlations to describe the behavior of a homogeneous poroelastic medium. After discussing the results, we concluded that for this sandstone, the best permeability constitutive correlation model is Walder and Nur.

Keywords: Poroelasticity; stress; permeability; simulation.

El flujo de fluidos y la mecánica de rocas se encuentran acoplados en varios fenómenos importantes en Geociencias. Con el fin de estudiar este acoplamiento, a lo largo de los años se han realizado trabajos de laboratorio en celdas triaxiales para diversos tipos de rocas y fluidos sometidos a diferentes esfuerzos de confinamiento y presiones de poro. Asimismo, también se han desarrollado modelos poromecánicos para simular dichas pruebas, para lo cual se requiere proporcionar correlaciones de la porosidad y permeabilidad en términos de deformación, esfuerzos y presión de poro. Sin embargo, hasta la fecha, todavía falta analizar la aplicabilidad de los modelos de correlación disponibles para describir este fenómeno en distintos tipos de roca. En este trabajo, se aplica un modelo poroelástico monofásico para simular una prueba geomecánica realizada en areniscas y tomada de la literatura, a fin de examinar la capacidad de las correlaciones constitutivas de permeabilidad y porosidad comúnmente utilizadas para describir el comportamiento de un medio poroelástico homogéneo. Después de discutir los resultados, se concluye que el mejor modelo de correlación constitutiva de permeabilidad para esta arenisca es Walder y Nur.

Descriptores: Poroelasticidad; esfuerzo; permeabilidad; simulación.

PACS: 91.60.Ba; 47.56.+r; 91.60.Np 07.05.Tp

1. Introduction

Fluid flow and rock mechanics become coupled in diverse important phenomena in Geosciences, such as underground water extraction, ground subsidence, CO_2 injection and depressurization of oil or geothermal reservoirs due to hydrocarbon or water steam exploitation. This non-linear coupling impacts the flow capacity of the porous medium due to stress-induced changes in the porous void structure, what becomes manifest by an alteration of the rock permeability. An illustrative simulation has shown, that the impact of non including this coupling in hydrocarbon recovery, is that an overestimation of about 10% of the total oil recovery in a reservoir can appear [1]. In order to study the flow-stress coupling phenomenon, laboratory work in triaxial cells has been worldwide performed along the time using cores of diverse rock types and structures, various fluids and diverse confining stresses and pore pressures [2–5]. It has been found that permeability changes result from a competitions between two mechanisms, (i) rock structure compaction that increases tortuosity and causes a decrease in permeability, and (ii) dilatation of voids, what increases pore volume and increments permeability [2]. In modeling this coupling, some constitutive corelationships between porosity and permeability in terms of stress depending properties should be provided. This correlations depend of the pore structure of the rock. In the case of sandstones, diverse empirical and theoretical correlations have been proposed [6–11], but an analysis of the applicability is not available in the literature. In this work, we employ a monophasic poroelastic model together with experimental results obtained from Jones and Smart [2] to study the capacity of diverse porosity and permeability constitutive correlations to describe experimental results. The paper is organized as follows. In Sec. 2 the mathematical an numerical model as well as its validation are presented. In Sec. 3 a description of diverse porosity and permeability constitutive correlations for grain structured porous media are presented. Further, in Sec. 4 an application of the model to the Jones and Smart experiment is shown, in which diverse constitutive relationships are employed, analyzed and discussed. Final remarks and conclusions are presented in Sec. 5.

2. Single phase flow poroelastic model

This model describes a single phase flow of a slightly compressible fluid in a porous medium with linear elastic deformation. The medium deformation is described by a quasi-steady-state moment equilibrium equation. The influence of the fluid is explained through the concept of effective stress

due to [12-14]. The total stress acting on a porous medium is partially supported by the solid matrix and partially supported by the saturating fluid. The effective stress represents the part of the total stress that is supported by the solid matrix and can be determined as a function of deformation.

The model considers an isothermal system composed by two phases, one fluid and one solid, each consisting of a single component. The solid phase is a deformable porous medium fully saturated by the fluid. The fluid is Newtonian and follows Darcy's law. Both, fluid and solid are slightly compressible. The solid phase is at rest, only displacements caused by mechanical stresses are present. Also, the solid has a linear elastic behavior and satisfies a Hooke's law for its constitutive stress-strain relationship.

2.1. Mathematical formulation

The poroelasticity equation system consist of a momentum and a mass balance equation derived by [12-14]. Here the model formulation follows Showalter notation [15].

The monophasic flow model in a deformable linear elastic porous medium is formulated as follows [14,16]:

$$\frac{\partial}{\partial t}(c_0 p + \alpha_B \nabla \cdot \boldsymbol{u}) - \nabla \cdot \left(\frac{\mathbf{k}}{\mu_f} \cdot \nabla p + \rho_f g \nabla z \right) = h_f \ , \quad (1)$$

where c_0 is the storage coefficient, p is the fluid pressure, also known as pore pressure, α_B is the Biot-Willis coefficient [17] ($0 \leq \alpha_B \leq 1$), $\boldsymbol{u}$ is the displacement vector, $\mathbf{k}$ is the absolute permeability tensor, μ_f is the fluid viscosity, ρ_f is the fluid density, g is the gravity aceleration, z is the elevation and h_f is the fluid source term.

The storage coefficient c_0 is defined as

$$c_0 = (\alpha_B - \phi) c_s + \phi c_f \quad (2)$$

where ϕ is the porosity, c_s is the solid grain compressibility and c_f is de fluid compressibility.

The quasi-stationary momentum balance equation for a porous medium saturated with a fluid is

$$-\nabla \cdot (\boldsymbol{\sigma}_e - \alpha_B p \boldsymbol{I}) = \rho_e g \nabla z \ , \quad (3)$$

where $\boldsymbol{\sigma}_T = \boldsymbol{\sigma}_e - \alpha_B p \boldsymbol{I}$ is the total stress tensor and $\boldsymbol{\sigma}_e$ is the effective stress tensor. While ρ_e is an effective or average density defined as $\phi \rho_f + (1-\phi)\rho_s$, being ρ_s the rock density.

In particular, the effective stress tensor according to Hooke's law for the linear homogenous and isotropic case can be expressed as

$$\boldsymbol{\sigma}_e = (\lambda + G) \nabla (\nabla \cdot \boldsymbol{u}) + G \nabla^2 \boldsymbol{u}. \quad (4)$$

where G and λ are the Lamé constants.

Note that porosity and absolute permeability tensor can be functions of the pore pressure (p), displacements ($\boldsymbol{u}$), volumetric strain (ε_v) or other quantities.

Here, the solid mechanics sign convention is considered, which means that compressive stresses are negative and tensile stresses are positive.

2.2. Initial and boundary value problem

The poroelasticity problem consists of Eqs. (1) and (3), and the unknowns are the pore pressure (p) and the displacement ($\boldsymbol{u}$). The initial and boundary conditions are:

Initial conditions

$$p(\boldsymbol{x}, t_0) = p_i(\boldsymbol{x}), \quad \forall \boldsymbol{x} \in \Omega, \quad t = t_0 \quad (5)$$

$$\boldsymbol{u}(\boldsymbol{x}, t_0) = \boldsymbol{u}_i(\boldsymbol{x}), \quad \forall \boldsymbol{x} \in \Omega, \quad t = t_0 \quad (6)$$

where p_i and $\boldsymbol{u}_i$ are initial values for pore pressure and displacement, respectively.

Boundary conditions

$$\boldsymbol{u}(\boldsymbol{x}, t) = \boldsymbol{u}_\partial(\boldsymbol{x}, t), \quad \forall \boldsymbol{x} \in \partial_D^u \Omega, \quad t > t_0 \quad (7)$$

$$\boldsymbol{\sigma}_T(\boldsymbol{x}, t) \cdot \boldsymbol{n} = \boldsymbol{T}_\partial(\boldsymbol{x}, t), \quad \forall \boldsymbol{x} \in \partial_N^u \Omega, \quad t > t_0 \quad (8)$$

$$p(\boldsymbol{x}, t) = p_\partial(\boldsymbol{x}, t), \quad \forall \boldsymbol{x} \in \partial_D^p \Omega, \quad t > t_0 \quad (9)$$

$$\boldsymbol{q}(\boldsymbol{x}, t) \cdot \boldsymbol{n} = \boldsymbol{q}_\partial(\boldsymbol{x}, t) \cdot \boldsymbol{n}, \quad \forall \boldsymbol{x} \in \partial_N^p \Omega, \quad t > t_0 \quad (10)$$

where $\boldsymbol{u}_\partial$, $\boldsymbol{T}_\partial$, p_∂ and $\boldsymbol{q}_\partial$ are the displacements, tractions, pressure and fluid flow at the boundary, respectively. Here, Ω is a bounded domain with boundary $\partial\Omega$ formed by two parts, one with Dirichlet conditions $\partial_D\Omega$ and another with Neumann conditions $\partial_N\Omega$, where $\partial\Omega = \partial_D\Omega \cup \partial_N\Omega$ and $\partial_D\Omega \cap \partial_N\Omega = \emptyset$.

The fluid flow is expressed by the Darcy's law

$$\boldsymbol{q} = -\frac{\mathbf{k}}{\mu_f} \cdot (\nabla p + \rho_f g \nabla z) \quad (11)$$

where $\boldsymbol{q}$ is the Darcy velocity.

2.3. Numerical discretization and computational implementation

All equations are discretized using a standard finite element method in space, and the Euler's backward finite difference method for discretization in time, what gives place to a full implicit scheme. The finite element method is applied with quadratic Lagrange elements in an unstructured triangular/tetrahedral mesh in 2D/3D. The resulting linear algebraic system is solved using the LU direct method UMFPACK for non symmetric and sparse matrices. The Newton-Raphson method is applied, since it is adequate for solving non linear problems.

The numerical model is implemented in COMSOL Multiphysics® using the module *PDE, Coefficient Form* [18].

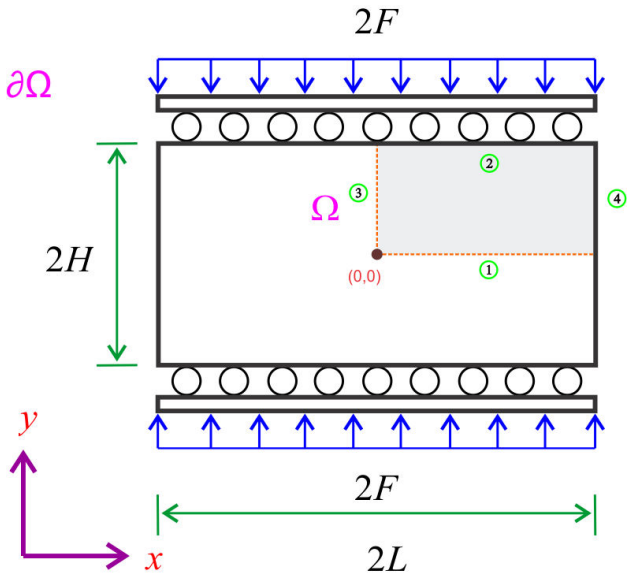

FIGURE 1. Mandel's problem domain and boundaries.

TABLE I. Mandel's problem data, taken from Ref. [21].

Property	Value	Unit
Drained Young modulus (E_d)	4.49E8	Pa
Undrained Poisson ratio (ν_u)	0.5	-
Drained Poisson ratio (ν_d)	0.0	-
Biot's coefficient (α_B)	1.0	-
Fluid compressibility (c_f)	4.0E-10	1/Pa
Solid grain compressibility (c_s)	0.0	1/Pa
Fluid density (ρ_f)	1000	kg/m^3
Porosity (ϕ)	0.25	-
Absolute permeability (k)	4.93E-14	m^2
Fluid viscosity (μ_f)	1.0E-3	Pa.s
Pressure at $x = L$ (p_{out})	0	Pa
Initial pressure (p_0)	0	Pa
Load at $y = H$ ($W = F/L$)	4.25E6	Pa

2.4. Model validation: Mandel's soil consolidation problem

Our model has been validated through the classical Mandel's consolidation problem [19]. This problem is commonly used to evaluate the precision of numerical solutions when a coupling between flow and geomechanical models is present, since an analytical solution of the problem is available [20].

Mandel's problem consists in the consolidation of a porous medium in 2D fully saturated by a fluid, which is placed between two impermeable rigid plates without friction, on which a compression force F is applied uniformly (see Fig. 1). In the system the lateral boundaries are of zero stress, allowing free fluid flow out of the domain Ω. Due to the symmetry of this problem, modeling is done only in a quarter of the domain, where all boundaries are non-flow except the right one (4) that is open to the flow at a constant pressure. The lower (1) and left (3) boundaries are restricted horizontal and vertical movement, respectively, while a uniform load is applied on the upper boundary (2), and the right boundary (4) is stress free.

Figure 1 shows the problem setting. The system domain is defined by $\Omega = [0, L] \times [0, H]$, where $L = 15$ ft and $H = 150$ ft. The domain is discretized by a regular mesh of 10×100 square elements.

2.4.1. *Problem data*

The data used in the Mandel's problem are taken from [21] and are displayed in Table I.

2.4.2. *Numerical versus analytical solutions*

The comparison of the numerical solution from COMSOL with respect to the analytical solution is displayed in Figs. 2 and 3, where the normalized pore pressure (p/W) and the displacement (u_x/L) profiles along the direction x/L at y/H = 0.5 for various dimensionless times t_d are shown. It can be seen that the discrepancy between the analytical and numerical solutions is pretty low. Indeed, the relative approximation error with respect to the infinite norm was estimated below 0.01 in all cases.

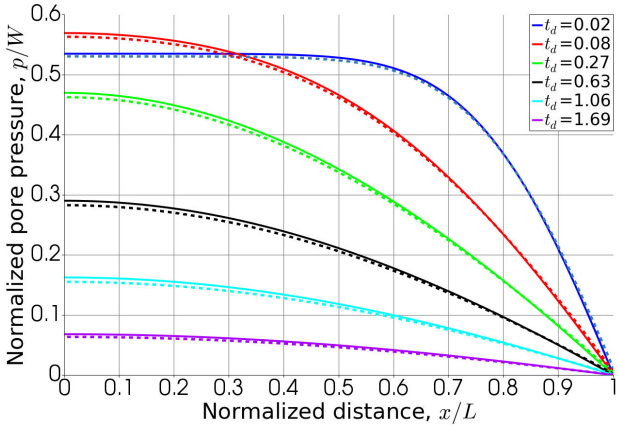

FIGURE 2. Normalized pore pressure profiles (p/W) along the direction x/L at y/H = 0.5 for certain dimensionless times t_d. The analytical solution (solid line), the numerical solutions (dotted line) are shown.

3. Porosity and permeability models

When a fluid is extracted or injected in a porous formation certain inherent properties such as porosity and permeability change. The factors that influence this change are among others, applied stresses, rock mechanical properties, fluid characteristics, temperature, etc. In order to be able to describe some of these changes, the equations in Sec. 2 must

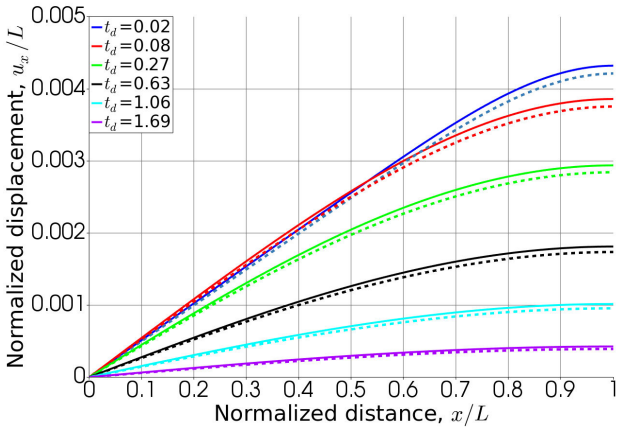

FIGURE 3. Displacement profiles u_x/L along the direction x/L at y/H = 0.5 for certain dimensionless times t_d. The analytical solution (solid line) and the numerical solution (dotted line) are displayed.

be solved together with some additional constitutive correlations, that provide porosity and permeability in term of quantities that characterize the mechanical state, such as local stress, volumetric deformation or fluid pressure. A long the time several theoretical and empirical models has been proposed [6, 8, 9, 22]. It is very important to mention that these constitutive correlations are not universal, they strongly depend on the type and structure of the rocks considered. Therefore some models will be more suited than others to describe the behavior of a particular rock. In this work, the capacity of the most commonly used constitutive correlations to reproduce experimental results is analyzed. Specifically, one fundamental model for porosity will be employed and four different permeability models will be tested. These correlation models involve the initial values for permeability (k_0) and porosity (ϕ_0) attained in equilibrium, just previous to the deformation process to be performed or described. It should be noticed that these values are not necessarily the laboratory values measured without any stress (k_R and ϕ_R). Further, it should be also noticed that the permeability correlation models have one or two parameters that depend on the characteristics of the porous structure, and in our work, they will be used as free parameters to fit the experimental results. Afterwards, the obtained fitting values are compared with data reported for specific rock types. If the fitting value is far outside the expected value, the model can be considered unappropriated for this specific rock type.

3.1. Porosity model

The porosity correlation model used here was proposed by Mainguy and Longuemare [23] and it is described by Coussy in his book [24]. It provides the porosity in terms of pressure and volumetric strain

$$\phi = \phi_0 + \alpha_B(\varepsilon_v - \varepsilon_{v0}) + c_s(\alpha_B - \phi_0)(p - p_0) \qquad (12)$$

where ϕ_0, ε_{v0} and p_0 are porosity, volumetric strain and pore presure at equilibrium, respectively.

3.2. Permeability models

By considering that a change in the rock porosity induces a change in the rock permeability, several authors have proposed different correlation models between these two dynamic properties. In this work we applied four well known constitutive correlation models to analyze the permeability behavior.

3.2.1. *Extended Kozeny-Carman correlation*

The Kozeny-Carman correlation model is one of the most widely accepted models that gives the permeability in terms of porosity power laws as

$$k = k_0 \frac{(1-\phi_0)^{b_1}}{\phi_0^{a_1}} \frac{\phi^{a_1}}{(1-\phi)^{b_1}}, \qquad (13)$$

where k is the rock permeability, k_0 and ϕ_0 are the equilibrium permeability and porosity, respectively, attained prior to the stress change process of interest. Parameters a_1 and b_1 depend on the porous material structure. The model has been theoretically derived by Carman [25] and Kozeny [26] by considering a uniform bed of spheres. In these works $a_1 = 3$ and $b_1 = 2$ were obtained. In other reports [27, 28] Chardabellas considered $a_1 = b_1 = B$, where B is a pore shape coefficient that ranges between 2 and 5.

3.2.2. *Walder and Nur correlation*

The Walder and Nur correlation model [29, 30] gives the permeability in terms of a power law of porosity, as

$$\frac{k}{k_0} = \left(\frac{\phi}{\phi_0}\right)^{a_2}, \qquad (14)$$

where a_2 is known as porosity sensitive exponent. The model has a theoretical origin supported by empirical data fitting [10, 35]. Suggested that this exponent ranges from 1 to 25 for common geological materials [31,32] give $a_2 = 11$ for a limestone. For Berea, Boise and Darley Dale sandstones a_2 ranges between 11.3 and 19.5 [33, 34].

3.2.3. *Touhidi-Baghini correlation*

This correlation model was proposed by Touhidi-Baghini based on theoretical considereations [27] and was adapted later by [28]. It gives the permeability in terms of the volumetric strain change as

$$k = k_0 \exp\left[\frac{a_3}{\phi_0}(\varepsilon_v - \varepsilon_{v,0})\right], \qquad (15)$$

where a_3 is a constant. Li *et al.* [27, 28] give for this constant a value of 5 in oil sands.

3.2.4. *David correlation*

This correlation model was proposed by [35] based on a previous work [36] and on experimental work with different sandstone types. This model considers an exponential dependence with stress and pore pressure. A similar expression is mentioned in the work by [37-40]. This correlation is written as

$$k = k_0 \exp\left\{-a_4\left[(\sigma_{zz} - \sigma_{zz,0}) - \alpha_B(p - p_0)\right]\right\} \quad (16)$$

where σ_{zz} and $\sigma_{zz,0}$ are the vertical stress and the equilibrium vertical stress respectively, and a_4 is a constant known as pressure sensitivity coefficient. David *et al.* [10,35] experimentally obtained that for some common sandstones (Boise, Fontainebleau, Berea, Adamswiller and Rothbach sandstones) this coefficient ranges from 0.0066 to 0.018 MPa^{-1}.

4. Application

The porosity and permeability constitutive correlation models from previous Sec. 3, valid for a homogeneous poroelastic medium, will be applied to describe the previously mentioned experiment by Jones and Smart [2]. This experiment was performed in a Hoek triaxial cell using a sandstone core subjected to a constant radial confining stress and an axial load that increases uniformly in time until rock failure. During the process a fluid is injected in the core to analyze the permeability reduction as function of the axial stress. Accordingly with the mathemical poroelastic model described in Sec. 2 only the elastic response region and monophasic fluid flow are examined in this work. Data obtained from the graphs displayed in Ref. 2 for differential stress and volumetric strain versus axial strain, and normalized permeability versus axial strain are used to test the mentioned constitutive correlations. Specifically, the free constant in each model (a_i) is used to fit the normalized permeability curve in the linear zone. The capacity of each model to reproduce experimental data is analyzed. Specifically, the fitting of permeability, volumetric strain and differential stress data as function of the axial strain is examined.

4.1. Experiment description

The Jones and Smart experiment [2] was performed in a set of Locharbrigg sandstone cores of 38mm diameter and 76mm lentgh, with 22.2 ± 0.6% porosity and 362 ± 82 mD permeability. The rock is strongly water wett (Amott index 0.91) and its compostion is 75% quartz, 15% feldelspar and 10% cement, made of clay and hematite. Of our interest is one of the four reported monophasic experiments. In this experiment the core is subjected to a constant radial confinement stress, $\sigma_2 = 21$ MPa (actually $3,000$ psi), and an axial stress, which initially is $\sigma_1 = \sigma_2$, and later increases linearly in time at constant rate of $6.66E-4$ s^{-1}, until the mechanical rock failure. During the process, a 5% NaCl-brine is injected at constant flow rate of 400 ml/h (6.7 ml/min), and produced at a constant output pressure of 1 atm. Graphical results of stress versus strain and volumetric strain versus strain are displayed in Ref. 2, and in the linear range are shown in our Figs. 7 and 8. At a strain lower than 0.5 % the curves show a linear elastic behavior with a reported Young's modulus of 14 GPa and a Poisson's ratio of 0.20. Also the resulting curve of normalized permeability as function of strain is given (in reality two similar cases from duplicated tests using equivalent rock samples are shown) [2]. At small strain values they show a linear reduction of permeability with increasing strain (see our Fig. 6). In this work the data from this linear region are used to fit the constitutive correlation models from Sec. 3.

4.2. Permeability models comparison

In this Section the mathematical and numerical model presented in Sec. 2 will be applied to the experiment described in the previous section using each one of the four permeability correlation models from Sec. 3.

4.2.1. *Simulation characteristics*

The problem is solved numerically by considering a 3D cylindrical domain $\mathbf{\Omega} = [0, R]$ x $[0, H]$, with $R = 19$ mm and $H = 76$ mm, using Cartesian coordinates x, y, z, as displayed in Fig. 4, and implementing the computational model described in Sec. 2.3.

The problem domain is discretized by an unstructured mesh of tetrahedral elements as shown in Fig. 5.

The experiment is modeled into two stages: (i) a first stage, where the core is subjected to a uniform hydrostatic stress of $3,000$ psi load on boundary 1, and same value of confining stress on boundary 3 (see Fig. 4). The boundary 2 (upper) is kept fix (without displacement), and boundaries 1,

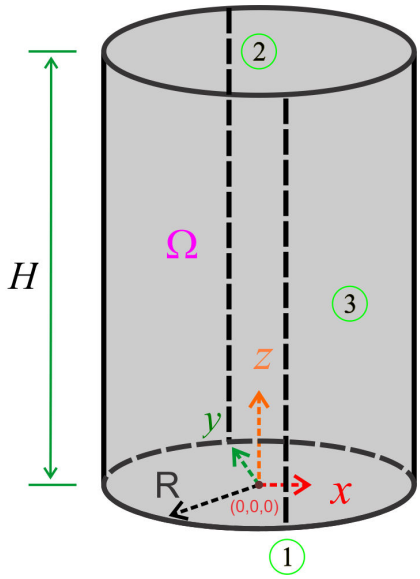

FIGURE 4.Cylindrical system domain used in the simulation, with radius R and height H and boundaries designed as 1 for the bottom, 2 for the top and 3 for the radial face.

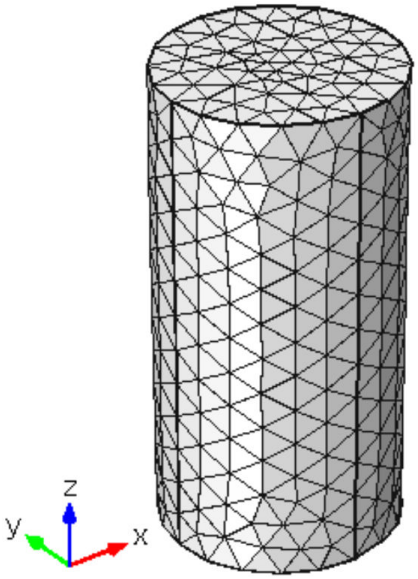

FIGURE 5. Mesh of 6,318 unstructured tetrahedral elements.

2 and 3 are assumed impermeable. From this first stage the equilibrium values k_0 and ϕ_0 are obtained. (ii) A second stage, in which a brine is injected through boundary 2 at a constant flow rate, and produced through boundary 1 at constant output pressure. Boundary 3 is impermeable to the flow. The axial stress on boundary 1 increases uniformly in time.

The data employed in the simulation were taken from Ref. 2 and are shown in Table II. The rock compressibility c_s, the Biot's constant α_B and other fluid and rock properties involved in the simulation are unknown for this specific case, but they were taken from typical or similar cases.

The procedure to determine the constants a_i involved in the constitutive correlation models considers a manual fitting of the experimental normalized permeability data, by a recursive systematic application of the numerical model. The experimental data are those from the upper curve of the normalized permeability versus strain plot in Ref. 2. Once the permeability is fitted, the obtained free parameter a_i value is compared against the corresponding value reported in the literature for equivalent sandstone rocks, and the accuracy of the correlation models to reproduce the experimental stress versus axial strain and volumetric strain versus axial strain curves is analyzed.

4.2.2. Permeability-axial strain dependence

After application of the previously mentioned permeability fitting procedure, the results obtained for each one of the correlation models are displayed in Fig. 6. The data are displayed as black dotes, and estimated experimental error lines corresponding to an average value of ± 0.05 are shown. They show a good match for all the correlation models (they all overlap). Three fitting cases of the Kozeny-Carman model are analyzed, as will be described below. The total RMS value is: 1.42E-3 for Kozeny-Carman model case (i), 1.94E-2

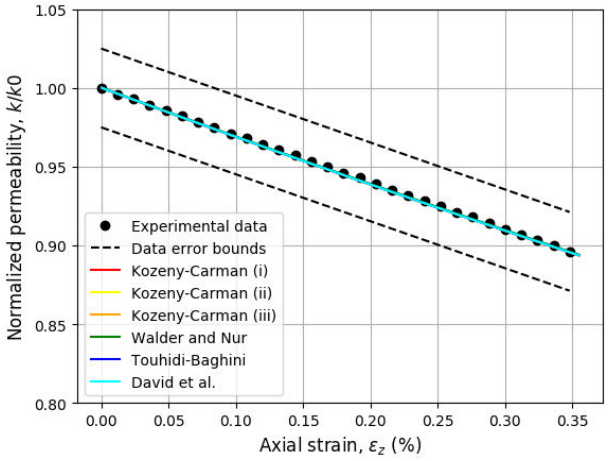

FIGURE 6. The change of permeability during axial compression. Data error range is ± 0.025. All correlation model curves overlap.

TABLE II. Experimental data used in the simulation.

Parameter	Value	Unit
Young modulus (E)	14.0	GPa
Drained Poisson's ratio (ν_d)	0.20	-
Biot's coefficient (α_B)	0.79	-
Solid grain compressibility (c_s)	2.7E-11	1/Pa
Fluid compressibility (c_f)	4.0E-10	1/Pa
Solid density (ρ_s)	2000	kg/m^3
Fluid density (ρ_f)	1000	kg/m^3
Rock porosity (ϕ_R)	0.222	-
Rock permeability (k_R)	362.0	mD
Fluid viscosity (μ_f)	1.0E-3	Pa·s
Production pressure (p_{out})	0.0	Pa
Initial pressure (p_0)	0.0	Pa
Constant flow injection rate (Q_{in})	400	ml/h
Initial stress (σ_0)	3000	psi
Axial load increase rate	6.66E-4	s^{-1}

for Kozeny-Carman model case (ii), 1.92E-2 for Kozeny-Carman model case (iii), 2.84E-3 for Walder and Nur model, 2.68E-3 for Touhidi-Baghini model, and 1.18E-3 for David *et al*. model. Accordingly to the Appendix, all correlation models can fit equally well the data since we are in the linear stress-strain and permeability-strain working region. Thus, the RMS value can not be used to evaluate the capacity of the models to reproduce the data.

The resulting fitted value for the free parameters are:

- The Kozeny-Carman correlation model was tested with three cases: (i) The situation in which $b_1 = 2$ was established and a_1 was optimized to reproduce the permeability data, it resulted $a_1 = 14.0$. The theoretical model predicts $a_1 = 3$. (ii) A second situation is by setting $a_1 = 3$ and let b_1 to be determined by optimization. It follows $b_1 = 41.45$, when the expected value is

2. (iii) The third situation is establishing $b_1 = a_1 = B$, and fits B. It yields $B = 11.41$. According with the findings [27,28] a valued of B between 2 and 5 was expected. Not an unique solution is available when both parameters a_1 and b_1 are simultaneously optimized.

- The optimization of the Walder and Nur correlation model yields $a_2 = 14.5$. This value falls inside the range expected for sandstones, between 11.3 and 19.5.

- The parameter fitting in the Touhidi-Baghini model yields $a_3 = 11.7$. The expected value for sandstones is 5.

- The optimization of the David et al. model gives $a_4 = 0.0022$ MPa^{-1}. The expected value is between 0.0066 and 0.018 MPa^{-1}. The value obtained is below the expected range.

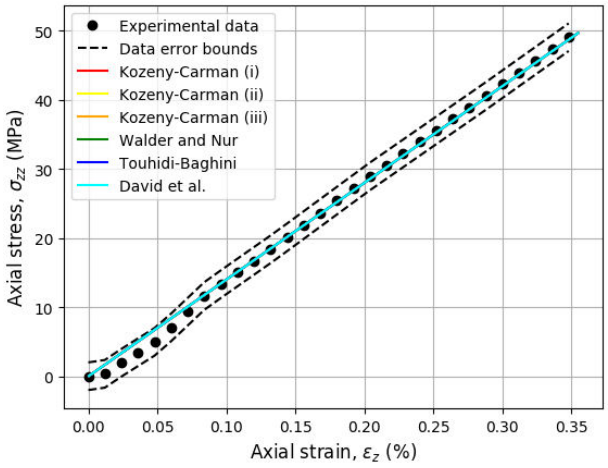

FIGURE 7. Axial stress vs. axial strain. Data error range is ±1.3 MPa. Note that all fitted correlation model give a straight line and overlap each other.

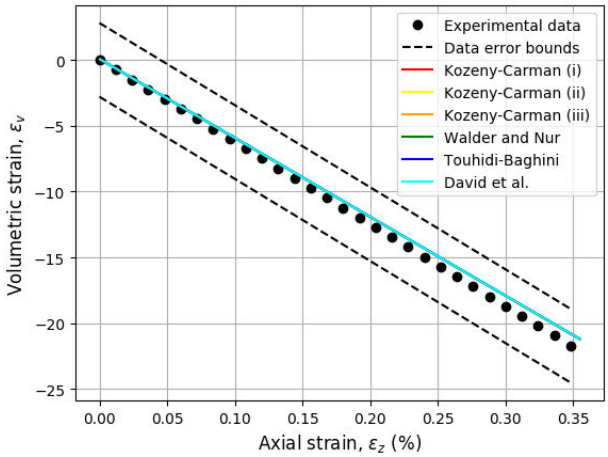

FIGURE 8. Volumetric strain vs. axial strain. Data error range is ±2.8. All curves models describe a straight line and overlap each other.

4.2.3. *Axial stress-axial strain dependence*

A plot of the axial stress as function of axial strain is provided in Fig. 7. All models describe a straight line and overlap each other. No better or worse correlation models appear from the fitting.

4.2.4. *Volumetric strain-axial strain dependence*

The simulation results of the volumetric strain as function of axial strain is provided in Fig. 8. Again, all models describe a straight line and overlap each other.

5. Final remarks and conclusions

The normalized permeability versus axial strain experimental data fitting yields equal results for the four permeability correlation models. This could be expected since we are analyzing the linear elastic region, as discussed in the Appendix. Thus, the RMS error values can not be used to determine which model results better. Also, the experimental axial stress versus axial strain, and volumetric strain versus axial strain data are equally well fitted by all four correlation models. The way that models can be discriminated is by comparing the obtained free parameter value against the expected value obtained by other authors from experimental studies in sandstones. Here, we found that the Walder and Nur correlation model provides the best description of the Jones and Smart's experiment on the Locharbriggs sandstone. It has to be mentioned that the correlation models are not universal, they are applicable to specific rock types and structures. Thus, we expect that more clear applicability differences will become apparent when working in the plastic non-linear stress-strain region, which is an area of future work.

Appendix A.

In this Appendix an analysis of the correlation models used in the work is presented. Specifically we explore their similarities and differences by performing a linearization on their volumetric strain and pore pressure dependence. This analysis helps in understanding the result similarities from the four permeability correlation models examined. The linearization yields:

- Mainguy and Longuemare correlation, Eq. (12), can be rewritten as a linear function of $\triangle X$ and $\triangle Y$

$$\phi = \phi_0 \left(1 + \triangle X + \triangle Y\right) \tag{A.1}$$

where $\triangle X \equiv (\alpha_B/\phi_0)(\varepsilon_v - \varepsilon_{v0})$ and $\triangle Y \equiv (c_s/\phi_0)(\alpha_B - \phi_0)(p - p_0)$ are dimensionless quantities, that presumably satisfy $\triangle X \ll 1$ and $\triangle Y \ll 1$, and $\phi_0 = \phi_R + \alpha_B \varepsilon_{v0} + c_s(\alpha_B - \phi_R)p_0$ is the equilibrium porosity.

- Extended Kozeny - Carman correlation can be approximated in terms of $\triangle X$ and $\triangle Y$ as follows

$$\frac{k}{k_0} \approx 1 + \frac{(a_1 + b_1\phi_0)}{(1 + b_1\phi_0)}(\triangle X + \triangle Y) \qquad \text{(A.2)}$$

where $k_0 = k_R(1-\phi_R)^{b_1}(\phi_0/\phi_R)^{a_1}(1+b_1\phi_0)$ is the equilibrium permeability.

- Walder and Nur correlation can be approximated in terms of $\triangle X$ and $\triangle Y$ as follows

$$\frac{k}{k_0} \approx 1 + a_2\,(\triangle X + \triangle Y) \qquad \text{(A.3)}$$

where $k_0 = k_R\,(\phi_0/\phi_R)^{a_2}$.

- Touhidi - Baghini correlation can be approximated by

$$\frac{k}{k_0} \approx 1 + \frac{a_3}{\phi_R}\frac{\phi_0}{\alpha_B}\triangle X \qquad \text{(A.4)}$$

where $k_0 = k_R \exp\left((a_3/\phi_R)\varepsilon_{v0}\right)$.

- Note that David correlation can be approximated in the same manner as Touhidi - Baghini correlation if σ_{zz} is expressed as function of vertical strain, *i.e.*, $\sigma_{zz} = E_d\varepsilon_{zz}$. Here E_d is the drained Young modulus.

In the case of the experiment described in this work we estimate ΔX and ΔY by using the data from Sec. 4.1 together with $\Delta\varepsilon_v = 0.03$ and $\Delta p = 120$ MPa. It follows $\Delta X = 0.11$ and $\Delta Y = 0.008$. Thus, the linear expressions obtained, Eqs. (A.2) to (A.4), for the correlation models are good approximations of the full expression presented in Sec. 3.

By analyzing the curves inside Fig. 6 we see that a linear behavior of permeability along a wide range of the strain is easily identified. Thus, it is to be noticed that all four correlations models can be described by a straight line that departs from $k/k_0 = 1$ and have a slope that depend on specific quantities, which involve a fitting parameter. Therefore, any model can fit the linear permeability experimental data as well as any other of the four models analyzed here.

Acknowledgements

This work is partially supported by the Fondo Sectorial Sener-Conacyt-Hidrocarburos through the Geomechanics Network Project 280097 in a joint collaboration between the Mexican Petroleum Institute, the University of Alberta and Pemex.

1. S. Ojagbohunmi, R. Chalaturnyk, and J. Leung, Coupling of Stress Dependent Relative Permeability and Reservoir Simulation. In *Eighteenth SPE Improved Oil Recovery Symposium held in Tulsa, Oklahoma, USA, 14–18 April 2012.*, SPE 154083. Society of Petroleum Engineers.
2. C. Jones, and B. Smart, Stress induced changes in two-phase permeability. In *SPE/ISRM Rock Mechanics Conference held in Irving, Texas, 20-23 October*, SPE/ISRM 78155. Society of Petroleum Engineers (2002).
3. F. Ma, S. He, H. Zhu, Q. Xie, and C. Jiao, The Effect of Stress and Pore Pressure on Formation Permeability of Ultra-Low-Permeability Reservoir. *Journal of Petroleum Science and Engineering*, **30** (2012) 1221-1231.
4. D. Huo, and S. M. Benson, Experimental Investigation of Stress-Dependency of Relative Permeability in Rock Fractures. *Transp Porous Med*, **113** (2016) 567-590.
5. B. Han, S. Y. Xie, and J. F. Shao, Experimental Investigation on Mechanical Behavior and Permeability Evolution of a Porous Limestone Under Compression. *Rock Mech Rock Eng*, **49** (2016) 3425-3435.
6. P. H. Nelson, Permeability-Porosity Relationships in Sedimentary Rocks. *The Log Analyst*, **35** (1994) 38-62.
7. T.F. Wong, and W. Zhu, Brittle faulting and permeability evolution: hydromechanical measurement, microstructural observation, and network modelling. *In Faults and sub-surface fluid flow in the shallow crust Geophysical Monograph* **113** (1999).
8. A. Costa, Permeability-porosity relationship: A reexamination of the Kozeny-Carman equation based on a fractal pore-space geometry assumption. *Geophysical Research Letters*, **33** (2006) 1-5.
9. Jia-Jyun Dong, *et al.*, Stress-dependence of the permeability and porosity of sandstone and shale from TCDP Hole-A. *International Journal of Rock Mechanics and Mining Sciences*, **47** (2010) 1141-1157.
10. J. Ma, Review of permeability evolution model for fractured porous media. *J. Rock Mech. Geotech. Eng*, **7** (2014) 351-357.
11. S.H. Gai, *et al.*, An improved particles model for stress sensitivity in low-permeability sandstones. *Geosystem Eng*, **19** (2014) 89–95.
12. K. Terzaghi, *Theoretical Soil Mechanics*. Wiley, (New York 1943).
13. M. A. Biot, General theory of three-dimensional consolidation. *Journal of Applied Physics*, **12** (1941) 155-164.
14. M. A. Biot, Theory of elasticity and consolidation for a porous anisotropic solid. *J. Appl. Phys.*, **26** (1955) 182-185.
15. R. E. Showalter, Diffusion in Poro-Elastic Media. (2000) p. 310-340.
16. Z. Chen, S. Lyons, and G. Qin, The mechanical behavior of poroelastic media saturated with a newtonian fluid derived via homogenization. *Internat. J. Numer. Anal. Modeling*, **1** (2004) 75-98.
17. M. Biot, and D. Willis, The elastic coefficients of the theory of consolidation. *J Appl Mech ASME*, **24** (1957) 594-601.

18. COMSOL Multiphysics, Reference manual, version 5.4. *COMSOL AB* (2018).
19. J. Mandel, Consolidation des sols (étude mathématique). *Geotechnique*, **30** (1953) 287-299.
20. Y. Abousleiman, A. H.-D. Cheng, L. Cui, E. Detournay, and J.-C. Roegiers, Mandel's problem revisited. *Geotechnique*, **46** (1996) 187-195.
21. A. Sangnimnuan, J. Li, and K. Wu, Development of efficiently coupled fluid-flow/geomechanics model to predict stress evolution in unconventional reservoirs with complex-fracture geometry. *SPE Journal* (2018) 640–660.
22. K. L. Kuhlman, and E. N. Matteo, Porosity and Permeability: Literature Review and Summary *Mechanical Behavior of Salt IX*, (2018) 15-27.
23. M. Mainguy, and P. Longuemare, Coupling Fluid Flow and Rock Mechanics: Formulations of the Partial Coupling Between Reservoir and Geomechanical Simulators. *Oil & Gas Science and Technology-revue De L Institut Francais Du Petrole - OIL GAS SCI TECHNOL*, **57** (2002) 355–367.
24. O. Coussy, *Poromechanics*. John Wiley and Sons, Chichester, England, first edition (2004).
25. P. C. Carman, Carman pc. fluid flow through granular beds. *Journal of Institution of Chemical Engineers*, **15** (1937) S32-S48.
26. J. Kozeny, Uber kapillare Leitung des Wassers im Boden, Sitzb. *Akad. Wiss. Wein, Math.-naturw Kl*, **136** (1927) 271–306.
27. A. Touhidi-Baghini, *Ph.D. thesis, Department of Civil Engineering, University of Alberta* (1998).
28. P. Li, R. Chalaturnyk, and M. Polikar, Issues With Reservoir Geomechanical Simulations of the SAGD Process. *Journal of Canadian Petroleum Technology - J CAN PETROL TECHNOL*, (2004) 43.
29. J. Walder, and A. Nur, Porosity reduction and crustal pore pressure development. *Journal of Geophysical Research: Solid Earth*, **89** (1984) 11539-11548.
30. S. Ghabezloo, J. Sulem, S. Guédon, and F. Martineau, Effective stress law for the permeability of a limestone. *International Journal of Rock Mechanics and Mining Sciences*, **46** (2009) 297-306.
31. S. Ghabezloo, J. Sulem, and J. Saint-Marc, Evaluation of a permeability?porosity relationship in a low-permeability creeping material using a single transient test. *International Journal of Rock Mechanics and Mining Sciences*, **46** (2009) 761-768.
32. S. Zhang, M. S. Paterson, and S. F. Cox, Porosity and permeability evolution during hot isostatic pressing of calcite aggregates. *Journal of Geophysical Research*, **99** (1994) 15,741–15,760.
33. W. Zhu, and T.-F. Wong, The transition from brittle faulting to cataclastic flow: Permeability evolution. *Journal of Geophysical Research: Solid Earth*, **102** (1997) 3027-3041.
34. Y. Bernabé, U. Mok, and B. Evans, Permeability-porosity Relationships in Rocks Subjected to Various Evolution Processes. *Pure and Applied Geophysics*, **160** (2003) 937-960.
35. C. David, T.-F. Wong, W. Zhu, and J. Zhang, Laboratory Measurement of Compaction-induced Permeability Change in Porous Rocks: Implications for the Generation and Maintenance of Pore Pressure Excess in the Crust. *PAGEOPH,*, **143** 425–456
36. J. R. Rice, Fault stress states, pore pressure distributions, and the weakness of the san andreas fault. *In: Fault mechanics and transport properties in rocks.*, (1992) 475-503. London, UK: Academic Press.
37. J. P. Evans, C. B. Forster, and J. V. Goddard, Permeability of fault-related rocks, and implications for hydraulic structure of fault zones. *Journal of Structural Geology*, 19:1393–1404. Department of Geology, Utah State University, Logan, UT 84322-4505, USA (1997).
38. C. A. Tang, L. G. Tham, P. K. K. Lee,T. H. Yang, and L. C. Li, Coupled analysis of flow, stress and damage (FSD) in rock failure. *International Journal of Rock Mechanics and Mining Sciences*, **39** 477-489. Department of Geology, Utah State University, Logan, UT 84322-4505, USA (2002).
39. J. Shafer, G. Boitnott, and T. Ewy, Effective stress laws for petrophysical rock properties . *Society of Petrophysicists and Well Log Analysts*, 1–15. SPWLA 49th Annual Logging Symposium held in Edinburgh, Scotland, May 25-28, (2008).
40. A. H.-D. Cheng, Poroelasticity. *Springer International Publishing*, (2016) 877.